SPACE Approach to Concrete's Space Structure and its Mechanical Properties

P. Stroeven
Faculty of Civil Engineering & Geosciences, Delft University of Technology, Delft

M. Stroeven
Faculty of Civil Engineering & Geosciences, Delft University of Technology, Delft
and Habanera, Delft

Structural properties of particulate materials can be described in densities of the particle packing, more generally denoted as particle composition. Obviously, this global measure does not offer information on the way particles are mutually arranged in space. This is associated with particle configuration. This terminology and the associated categories of material behaviour that rely on either one of these extremes of structural properties are elaborated in this paper. The range of such properties will be between structure-insensitive ones, like mass or stiffness (Young's modulus), and structure-sensitive properties like crack initiation and tensile strength.
The establishment of an experimental basis for the dependence of a mechanical property on certain structural features (and the associated micro-mechanical properties) would require extensive, cumbersome and complicated testing: mechanical testing for defining the very property, quantitative (section) image analysis and stereological three-dimensional assessment of the relevant structural features. 'Realistic' simulation of material structure by computer would therefore offer an interesting alternative. This paper introduces the SPACE system (Software Package for the Assessment of Compositional Evolution) as the most recent development in this field. It has been developed to assess the composition as well as configuration characteristics of dense random packing situations in opaque materials. This paper presents an introduction to the system and will thereupon highlight by means of illustrative examples of typical applications on different levels of the microstructure the system's capabilities. Although only a single application can be presented in this framework, they all concern areas of major engineering interest.

Keywords: **Composition, configuration, interfacial transition zone, material model, particle packing, SPACE, stereology, structure-sensitivity.**

1. Introduction

Cementitious materials can be considered consisting of particulate elements on the various levels of the microstructure. In an ordered fashion, they build up a crystalline structure in the hydrated state. The binder particles in fresh concrete form on microlevel the so-called matrix. When matured, the matrix stabilises the skeleton of aggregate particles on meso-level. To realistically simulate this densely packed particulate matter, the common simulation methods based on so called 'random generators' (RG-systems) will reveal serious limitations. Particles of a certain range of particles sizes are sequentially positioned inside a container by RG-systems. Each location is 'randomly' generated. With such high

densities as met in this category of problems, 'overlap' will occur to an increasing degree during the generation process. The solution is to reject such overlap situations, whereupon the generation process is continued. Obviously, 'dense random packings' can not easily be generated in this way. So, this approach is *unpractical* due to the excessive computer time requirements at high particle densities. Moreover, a more uniform structure is obtained, under-estimating a natural phenomenon such as clustering of particles. As a consequence, the results are *unreliable*, because the rejection procedure leads to biases in particle configuration that are dramatically increasing with particle density [1]. Therefore, a more realistic computer system for simulating particulate materials would be appropriate, particularly for studying structure-sensitive properties of such materials.

After World War II, the awareness grew that the material structure exerted a major influence on mechanical behaviour of concrete. This was evidenced by increased research interest that resulted in a large number of publications issued since the sixties. As an example, reference should be given to those dealing with extensive and concentrated research performed at Cornell University [2] and at Imperial College [3,4]. Computer simulation of damage evolution by finite element approaches started in the seventies, an example being the so-called 'numerical concrete' [5]. Sections of concrete specimens with a low areal content of *randomly dispersed* multi-facet particle sections were used for this purpose. The serious drawbacks of random generation methods to correctly reproduce actual conditions in cementitious materials asked for more 'realistic' approaches, however. Our first efforts to do so go back a quarter of a century; the idea of a 'dynamic' stage was implemented in a computer simulation system of particulate matter that was developed *halfway the 1970s.*

The simulation started from a Poisson field of points inside a container. The points served as nuclei for programmed particle growth, leading to a particulate system governed by a particular size distribution function (or sieve curve). Overlap was eliminated by agglomeration rules. One of the fully elaborated rules was particle 'sintering'. This implied that once in contact, the clustered particles continued to grow from their common centre of gravity, thereby destroying the initial state of randomness to an ever increasing degree. The resulting maximum particle densities were relatively low, however, in this dynamic simulation system. Nevertheless, it was shown that the actual dispersion of the sieve fraction of largest particles in a concrete mix (ceramic spheres were employed in the experiments for discrimination purposes) was better simulated by this system than by a random generator-based one. Generally, the simulated material was composed of spherical particles of different size that at final (designed) density yielded the successive particle fractions (such as 4, 8 and 16 mm) of a so-called Fuller mixture. As an example, the extension of a (due to particle clustering) disturbed boundary layer of a 100 mm model concrete cube was assessed at increasing particle volume densities, and found to increase disproportional with volume fraction [6].

Figure 1 is another (historical) example revealing the number of particles, N_C, in contact in the 'unbiased' central part of the cube (resulting after removal of the biased boundary layer) as a percentage of the total number of particles in the cube, N_T: clustering is shown to be a natural phenomenon starting already at low volume fractions.

The second agglomeration rule was frictionless sliding of particles-in-contact. This would be more representative for aggregate in higher slump concretes, or cement particles in superplasticized pastes. This allowed reaching much higher particle densities.

A new start was made in a PhD study during the *1980s* with the development of a more advanced dynamic computer simulation system for particulate materials. The idea was to simulate the production process of the material (in the case of concrete: mixing of aggregates, water and cement). A mixture could consist of spherical or polyhedron-shaped particles (simulating aggregate of fluvial origin and of crushed rock, respectively) and

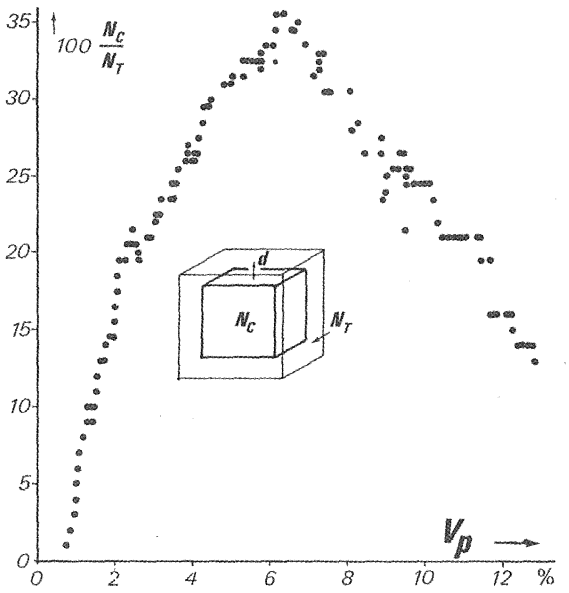

Figure 1: *Multi-sized system of growing particles (sintering mechanism); number of particles in contact in the unbiased central cube, N_C, is plotted as percentage of the total number of particles, N_T.*

fibres [7]. The container was imaginary subdivided into a large number of cubical spaces to which particles were attributed at random, so that initial overlap was automatically avoided. Fibres were added in a second stage. Next, all elements in a mixture of particles and fibres were set to move as a result of attributed forces, and to collide as rigid bodies. By adding a force component directed to the centre of the container, the element density could be made to gradually increase. During this process, also the container size was reduced. The irregularly-shaped aggregate particles were replaced during this densification process by spherical ones of which the diameter was equal to the maximum dimension of the replaced particle. Only in a final densification stage this simplification condition was lifted, to avoid cumbersome calculations for overlap assessment during the full densification process. This system was employed, among other things, for studying the dependence on the aggregate composition of the fibre reinforcement efficiency in the boundary zone of fibre reinforced concrete elements [7,8].
A final start could be made during the *mid-1990s* in the framework of a PhD study of the second author. This resulted in the development of the newest version of the dynamic computer simulation system with the acronym SPACE (*i.e.* Software Package for the Assessment of Compositional Evolution) The capabilities of the system will be illustrated by three applications in different fields of engineering interest. These illustrative applications will deal with

- **optimisation of aggregate composition in concrete**.
  Hence, this is an application on *macro-level*, whereby representative quantities of the different sieve fractions of the aggregate are concerned.
- **characterisation of the interfacial transition zone in concrete**.
  This is an application on *micro-level*, dealing with the packing structure of binder

particles in the fresh state (an hydration algorithm is available for studying the structural changes during this hardening process).

- **simulation of crack development in concrete.**
  This is an application on *meso-level*. A number of simulated concrete specimen are subjected to a finite element simulation.

2. Simulation system SPACE

The non-homogeneous, or granular, nature of the internal material structure is represented by a set of *distinct elements*. Each element corresponds to a distinguishable, characteristic phase in the material. For example, concrete is modelled as a set of elements representing the aggregate particles. The elements are dispersed in a presumably homogeneous mortar matrix moulded in a container. Similarly, cement paste is modelled as a set of elements representing cement particles dispersed in water. The parameters describing the static conditions of the internal structure are the locations, orientations, and shapes of the various individual elements. Since the elements represent real physical phases in the material, physical properties can be assigned to each element along with its shape and size, at least *in principle*. The most difficult task, however, is the derivation of the location and the orientation of these non-overlapping elements.

2.1 Static Simulation of Particle Positions

In a static simulation system, the particles will be sequentially located inside a container. Each location is governed by randomly generated co-ordinates. 'Overlap' with earlier generated particles will result in rejection, whereupon the generation process is continued. The number of rejections will increase dramatically at high volume fractions, making the generation process very time-consuming, if not impossible at all in the highest density range. Simulation of a multi-size particle composite requires starting with the largest particles in the mix. The system obviously excludes the mechanism of *mutual particle interaction*, which is so characteristic for the production stage of cementitious materials. The re-generation after rejection inevitably leads to an under-estimation of a natural phenomenon as particle clustering. The generated nearest neighbour distribution of the particles will reveal, as a consequence, dramatically large biases at higher particle densities [10]. Three of the more popular systems in this category were developed by Roelfstra [11], by Diekkämper [12], and at NIST [13]. An example of a statically simulated material structure is given on the left hand side of Figure 2.

2.2 Dynamic Simulation of Particle Positions

The SPACE system is based on a dynamic concept of simulating the production process of composite materials, *i.e.*, in case of concrete: mixing of aggregates and paste, or cement and water. The details of the generation system have been published by the authors elsewhere [1,9]. To be able to simulate effects such as clustering and to reach high volume densities, element motion and inter-element collision are modelled [14], leading to effective ingredient mixing. This stage is referred to as the *dynamic stage*.
The general simulation concept can be described as follows:

- Initially, a structured or random 3-D *dilute* distribution of elements is generated within the boundaries of a container, using the static 'rejection' mechanism mentioned earlier. So far, only spherical particles can be conceived by SPACE. Next, random linear and rotational velocity vectors are assigned to each element.
- The second step, the actual dynamic stage, is an iterative procedure where location and orientation of all elements are changed at each time step according to a

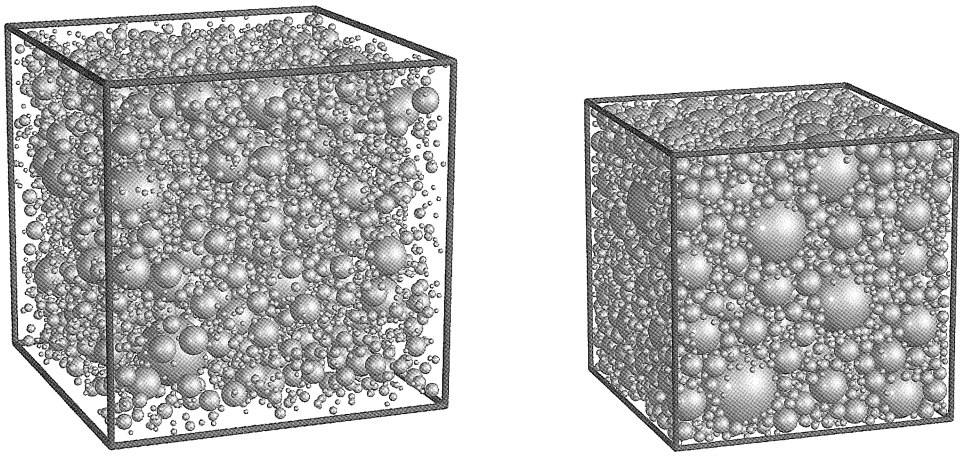

Figure 2: *Example of a 3D material structure* ***(left)*** *after the static simulation and* ***(right)*** *after the dynamic densification process*

Newtonian *motion model*. This motion model relates the element's linear and angular displacement to a set of conditions enforced on the element (*e.g.*, gravity, friction, etc.). When elements meet during this time interval, a *contact model* defines the effect of contact on the motion/rotation update. Inter-particle influences - one of the requirements for achieving a more versatile system - are incorporated in the *contact model*. Additionally, electrical or chemical inter-particle forces may be added to the *motion model*. This will allow to more accurately adjust SPACE simulations to the particle aggregation conditions (*i.e.* flocculation) of the fresh cement paste. In the present concept, the use of this facility was considered to needless complicate matters, because no quantitative estimation of the ITZ thickness was pursued. The density can be varied during this stage by gradually moving the container walls towards eachother (compaction) or away from eachother, or by applying a gravitational force.

- Finally, the iteration stops when certain conditions are reached, such as the relevant volume fraction of aggregate, or the required water to cement ratio (W/C ratio).

The final distribution state can incorporate effects due to gravity and to inter-particle influences. Simple physical laws may be used to define the inter-particle relationships, by introducing parameters such as specific mass and energy dissipation. Maximum packing densities can easily be simulated by the SPACE system. Such densities are relevant for aggregate packing problems on engineering level, or for binder particle packing problems particularly at low water to cement ratios, appropriate for High Strength or High Performance Concrete systems. A densily packed material structure is shown on the right hand side of Figure 2 which is the results of the dynamic compaction of the structure displayed on the left hand side of Figure 2.
It should be noted finally, that the dynamic stage is a built-in mechanism to achieve high densities that can not be realised by static simulation systems. The dynamic stage is supposed to imitate, moreover, the production stage of the material. All forces added to the system can be manipulated, so that 'sticky' particle contacts during the production of the model material can also be simulated. *The dynamic (Newtonian) simulation mechanism has no significance after completion of the simulation, hence, is not connected with the rheological properties of the model material.* Once mixed, the aggregated cement particles constitute a

static system that is the basis for application of the hydration algorithm.

2.3 Hydration Process

The hydration process will be outlined in two steps. First, the representation of a hydrating cement particle as a set of concentric spheres will be clarified based on the hydration description of a single particle. This description largely follows the hydration description presented by van Breugel in [15]. Second, the more complicated situation of multiple merging particles will be evaluated.

Hydration of a single cement particle

The kinetic hydration process of a single particle consists of two subsequent stages in time. The first stage, in which a phase-boundary mechanism controls the hydration rate, is followed by a stage in which the reaction rate is controlled by a diffusion mechanism. The transition between the two stages is assumed to occur when the thickness of the layer of the reaction product $d(t)$, precipitated on the cement particle at time t, equals a transition thickness δ_{tr}. The inward growth or decrease Δr_{in} of the unhydrated cement surface for a sufficiently small time period Δt is then given by

$$\Delta r_{\text{in}} = \Delta t \, K_0 \left(\left(\frac{\delta_{\text{tr}}}{d(t)} \right)^{\beta} \right)^{\gamma} \tag{1}$$

where K_0 is the rate constant, $\gamma = 0$ as long as $\delta_{\text{tr}} > d(t)$ and $\gamma = 1$ otherwise. The constant β regulates the diffusion process. The chemical reaction between cement and water results in a gel-product. The relationship between the volume change ΔV_{in} of the hydrated cement and the volume change ΔV_{out} of the gel or outer product is given by

$$\Delta V_{\text{out}} = v \, \Delta V_{\text{in}} \tag{2}$$

with constant $v = 2.2$ [15]. A volume of ΔV_{in} of the reaction product is used to fill the space of the reacted cement. The remaining volume precipitates equally on the existing gel surface of the particle thereby introducing an outward growth. In this simulation the water will appear in three forms, *i.e.* chemical water, which is chemically bound to the cement by the hydration reaction, physical water which is adsorbed in the pores of the gel, and free water, which is supposed to be the only form available for hydration. At initiation all water is free. An amount of water of 25% of the weight of the cement is chemically bound, and an amount of 15% by weight is physically bound. Consequently, a reacted volume of V_{in} cement requires a volume of water equal to

$$\Delta V_{\text{fw}} = 0.4 \, \rho_c \, \Delta V_{\text{in}} \tag{3}$$

Herein $\rho_c = 3.1$ $[g/\text{cm}^3]$ represents the volumetric density of cement. Since the volume of the reaction product is smaller than the total volume of reacted cement and water, a fourth phase is introduced, air. Again, the reduction of the water supply occurs on the surface of the air-water interface, causing an outward growth of the air layer. The modelling of an air layer around a particle is merely used to keep track of the *local* amount of water that has been used by that particle. It does *not* represent the actual location of the air. The deposition of the gel product, and the consumption of cement and of free water is assumed to be equally divided over the entire surface. Thus the cement-gel interface as well as the gel-air and air-water interfaces remain located on concentric spheres throughout the hydration process (see Figure 3 (left)). As a result, a formula can be given that relates the volume change Δ_{x} of a chemical product x that has a surface radius of r_{x} to its radial change Δr_{x} by

$$\frac{4}{3}\pi[(r_{\text{x}} + \Delta r_{\text{x}})^3 - r_{\text{x}}^3] = \Delta V_{\text{x}} \qquad \text{for} \qquad \text{x = in, out, fw} \tag{4}$$

This is particularly convenient for modelling purposes. The product thickness $d(t)$ in eq. (1) is thus given by $r_{\text{out}} - r_{\text{in}}$. It should be noted that the formation of an air layer around the gel in the model is merely used to accommodate for the local consumption of water. It is not intended to represent the actual location of air. It is assumed that if water is still available (*i.e.* there exists an air-water interface) it will be equally available for the entire cement surface, hence causing a concentric decrease of the cement core. Note that at $t = 0$, $r_{\text{in}} = r_{\text{out}} = r_{\text{fw}}$, and at $t > 0$, $r_{\text{in}} \leq r_{\text{out}} \leq r_{\text{fw}}$. In brief, eq. (1) yields the decrement of r_{in} per time step Δt, whereupon new values of r_{out} and r_{fw} can be obtained using eqs. (2) and (3). This rather simple model holds as long as particles do not make contact and water does not run out.

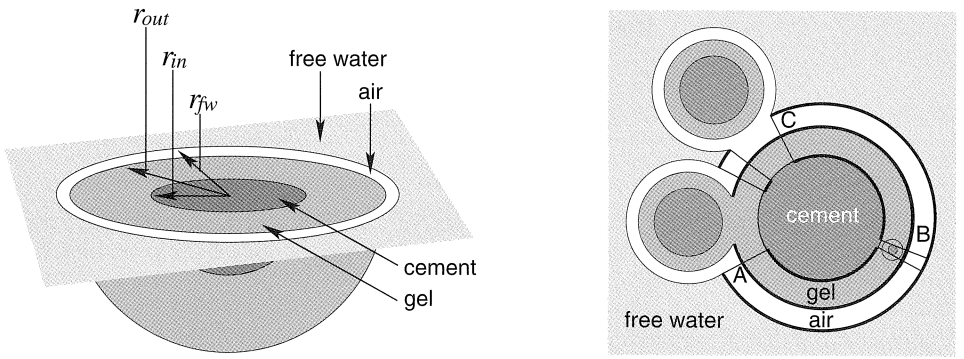

Figure 3: ***(left)*** *Geometrical representation of hydrated cement and* ***(right)*** *various contact situations between cement particles.*

Hydration of multiple cement particles
However, the simultaneous expansion of other particles in the vicinity will have the following severe effects on the hydration behaviour:

- growing contact areas between the gel products of neighbouring particles diminishes the surface area that is available for product deposition. Figure 3 (right) illustrates a two dimensional representation of this situation, whereby the thick line at the gel-air interface represents the free surface onto which the gel product may precipitate. Less surface area signifies a thicker deposit of the product layer.
- similarly, the consumption of water can only occur at the interface between air and free water (represented in Figure 3 (right) by the thick line at the air-water interface).
- the influences of contact on the inward growth of the cement is more complicated. A particle embedded in the gel layer, as illustrated in Figure 3 (right) - case B, prevents part of the gel surface to be active in the diffusion process. Moreover, the inward growth is also influenced by the reduction of free water (Figure 3 (right) - case C).

Let A_{fw} be the surface area of a sphere with radius r_{fw}, then $\omega_3 A_{\text{fw}}$ corresponds to the total air-water surface and $\omega_2 A_{\text{out}}$ equals the total gel-air surface. The factor ω_1 corresponds to the fraction of the total surface area that is active in the hydration process. The shielding effect as well as the water reduction are accounted for in ω_1. In the next section the values of ω_1, ω_2 and ω_3 will be evaluated.

Surface tessellation
To efficiently evaluate the free surface of a sphere an algorithm has been implemented that divides the surface in triangular tesserae, or surface patches as show in Figure 4. By using

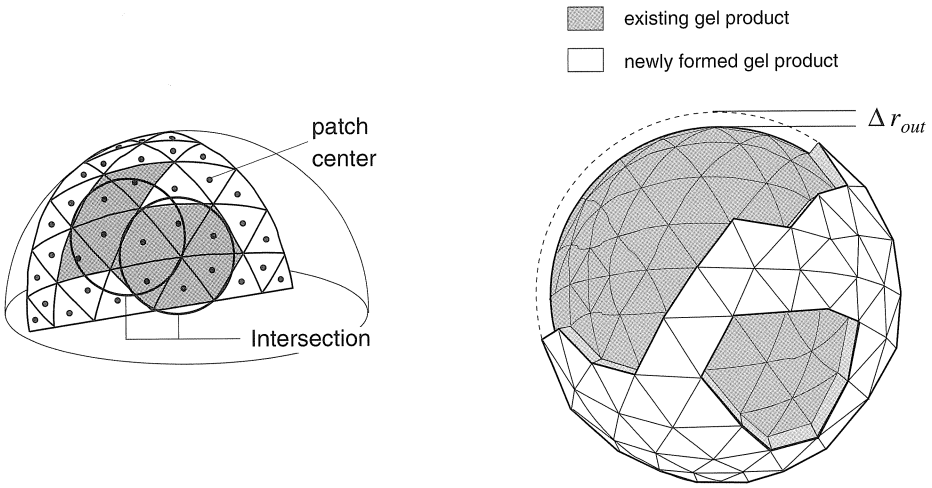

Figure 4: *Partly tessellated sphere surface of low order k. Grey area denotes the detected surface that is contained by one of the two spheres of which only the circular intersections are shown.*

an algorithm that generates a pentakisdodecahedron [16] of order k, the surface will be divided into $N = 2 \cdot 4^k$ surface patches of which only the centres are stored. It should be mentioned that the location of a specific point only changes in radial direction when the size of the sphere is altered. The fraction of the total spherical surface of the object that is not contained by any other object can now simply be determined by

$$\omega = \frac{n}{N} \tag{5}$$

in which n corresponds to N minus the number of patch centres that are contained by an arbitrary other sphere. As an example Figure 4 shows the circular intersections of a sphere with two other (fused) spheres and the 10 detected surface patches that are contained by these spheres. The correction factor ω_3 of an object can now be obtained by counting the number of free surface patches n_3 when the size of each particle is temporarily changed to the radius of its own free water intersection (r_{fw}). Substitution of n_3 into eq. (5) yields the required correction factor. The same calculation, but now with the size altered to r_{out}, yields the correction factor ω_2. The correction factor ω_1 is determined in two steps. At first the total number of sphere patches N that are active in the diffusion process is reduced by n_3 to accommodate for the water reduction (cases A and C of Figure 3 (right)). Secondly, it is checked whether the corresponding point on the gel-air surface of each remaining free surface point had been inactive during an earlier hydration stage. If so, they are considered inactive too. This operation imitates the shielding effect of particles that are partly embedded in the gel (case B of Figure 3 (right)). To conclude, an iterative repetition of the following procedure implements the hydration process

1. Determine Δr_{in} according to eq. (1). Calculate the volume change ΔV_{in} when only a fraction ω_1 of the cement surface hydrates. Calculate a new value for the inward growth $\Delta r'_{\text{in}}$ when a concentric decrease is assumed.
2. Determine ΔV_{out} using eq. (2) and calculate the outward growth when precipitation only occurs on a fraction ω_2 of the surface A_{out} (see Figure 4 (right))

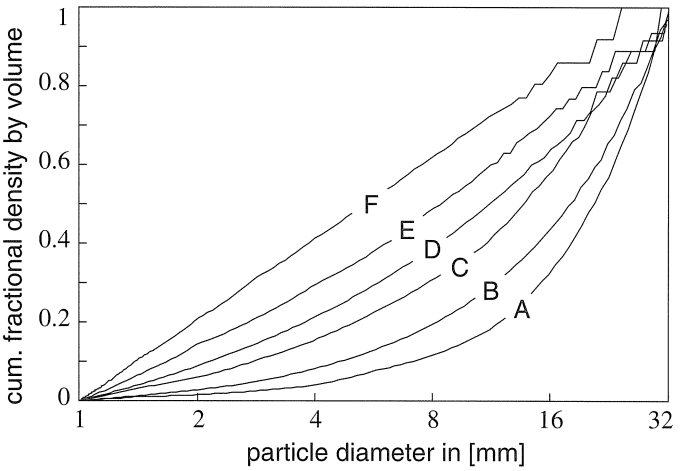

Figure 5: *Cumulative particle size distribution function for particles between 1 and 32 mm on a semi-logarithmic scale. The functions represented by the solid lines correspond to the numerical mixtures, whereas the values indicated by the circular dots refer to the measured values of the experimental mixtures.*

3. Determine ΔV_{fw} using the relationship in eq. (3) and calculate Δr_{fw} when water is only consumed from the surface area $\omega_3 A_{\mathrm{air}}$.

3. Particle packing on macro-level

One of the features of the SPACE system is the capability to densify the structure during the mixing process. This option is frequently used to obtain a particular density for a mixture, which cannot always easily be obtained by random generation methods. The question could now be posed whether the densification method could be applied as well for the estimation of the ultimate density of a mixture with a given particle size distribution function or sieve curve.
A series of experiments were performed in which six different mixtures (A—F) each consisting of 15,000 particles were generated by the SPACE system and densified up to their ultimate density. The solid lines in Figure 5 refer to the cumulative size distribution functions of these aggregates. Additionally, six gravel/sand mixtures were experimentally densified, of which the corresponding cumulative fractional density values are indicated in Figure 5 by the circular dots. Note that the numerical size distribution graphs contain more information on the particle mixtures than a sieve curve which is based on a very limited number of sieve opening sizes only. Curves C and F roughly correspond to the limits of the sieve curve area in the Dutch building code (NEN 2560). Of the intermediate mixes, D corresponds to the Fuller curve.
Of course, expectations on correspondence between outcomes of experiments and simulations cannot run too high, because of inevitable differences between both approaches. First of all, it is well-known that among the various experimental methods to evaluate maximum packing density of aggregates, experimental results will vary significantly [20]. But the conditions can be varied even for one particular method, thereby additionally influencing the outcomes. In the present case, use was made of an 8 litre cylindrical container, in which the mixture of dry sand and gravel particles was compacted for 10 seconds. So, at least the container size can be added to the factors having influenced

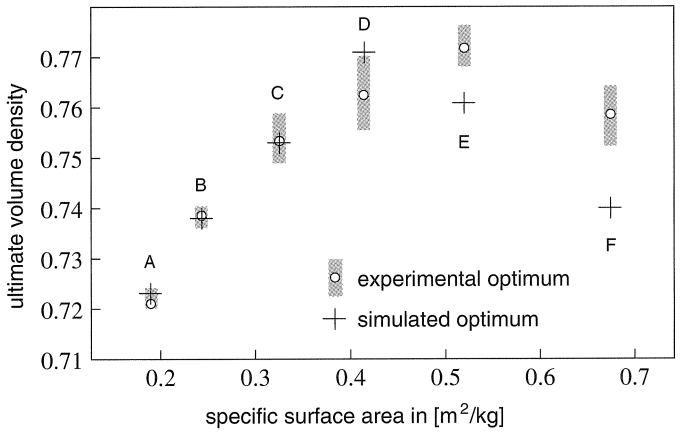

Figure 6: *Simulated and experimental values of maximum density of the mixes indicated in Figure 5 plotted as a function of the specific surface area; particle size ranges from 1 to 32 mm.*

the experimental data. On the computer side, periodic boundaries were selected for correctly simulating *bulk* characteristics. In the iterative procedures of the earlier described dynamic stage of the SPACE system, some particle overlap is only a temporary feature. A certain amount of *residual* overlap has to be accepted, however, when maximum density is approached. In the present case, the acceptance level was set at 1% overlap by volume, a choice influencing the simulation outcomes. Obvious differences between the two approaches further concern the particle shape (spherical in the simulation), and the particle size distribution curve (the sieve curve underlying the experiments is well-known to only poorly reflect the actual size distribution of the particles [21]).

Together with the experimental data, the outcomes of the simulation are plotted in Figure 6 as a function of the fineness modulus. Figure 6 reveals for both approaches the highest density to be obtained for mix E, 'somewhere halfway' between Fuller and equal volume fraction curves (on semi-logarithmic scale), a result of practical significance. Maximum volume density increases with declining fineness modulus from mix A to mix E. After passing this optimum, a drop occurs from mix E to mix F. In the light of the foregoing, the agreement between simulated and experimental outcomes can be considered *very satisfactory*. These tendencies are accompanied by characteristic changes in the underlying particulate structure. As an example, Figure 7 visualises these differences in structure by way of section images of simulated mixes B and F, which have (about) the same density ($\approx$0.74).

The second step in trying to assess volume density of sand/gravel mixes by the SPACE system is going from densified 'gravel' to 'densified gravel and sand'. The last problem would involve extending the particle size range to the micrometer level. Aggregates with such a wide range of particle sizes cannot be dealt with realistically, because of the excessive number of particles involved. But the problem can be approached in a qualitative way. It is demonstrated by Figure 7 that curve B leads to dispersed 'pores' between the particles, that are larger than those in mix F. This is due to the larger number of small particles in the latter case, which subdivide the open space into smaller pores. These smaller pores are less easily accessible by the sand without increase in overall volume. Hence, of the two, curve B should lead to higher densities after mixing with the sand. SPACE is used partly in a quantitative and partly in a qualitative sense to estimate the

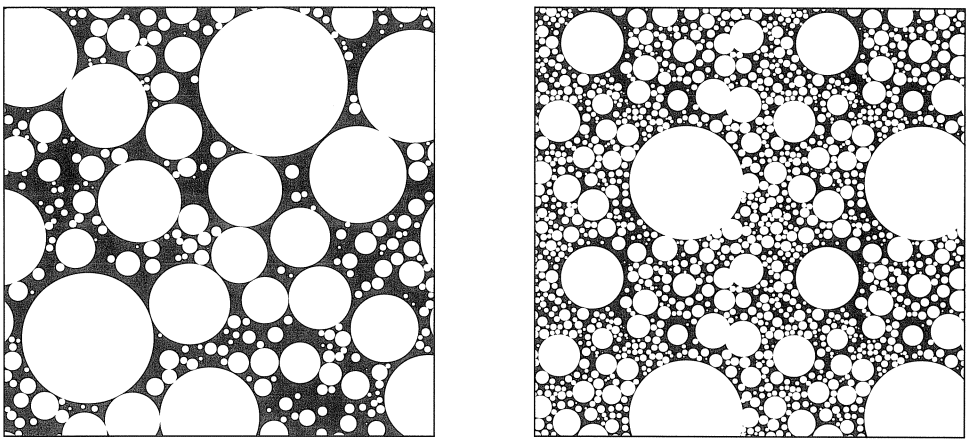

Figure 7: *Sections of the compacted particle mixtures* B ***(left)*** *and* F ***(right)*** *defined in Figure 5; significant differences in details of the packing structure are visible despite an almost similar total volume density of 0.74.*

sand-accumulation capacity of the gravel at optimum density. For additional details, see [22].

4. Particle packing on micro-level

The paramount interest in the Interfacial Transition Zone (ITZ) in cementitious composites is derived from the recognition that in normal concretes the ITZ constitutes the weakest link in the mechanical system. Hence, methods for upgrading concrete into the high strength or even high performance ranges should be in the first place effective in disproportionately improving the 'quality' of the ITZ [23]. In doing so, the impact of the ITZ on material performance can be eliminated, leading to high strength but also to extreme brittleness. A significant reduction in the water to cement ratio, rendered possible by the use of a superplasticizer, has been demonstrated as a way in achieving this goal. Increasing the range of particle sizes in the binder by adding fine-ground fly ash or rice husk ash, also works out favourably [24]. The underlying particle packing mechanism is strongly reinforced by adding the much finer silica fume, leading to DSP-(Densified with Small Particles)-Concrete. Almost the same mechanical effects were obtained by replacing these pozzolanic particles by inert ones of similar fineness (*i.e.* of carbon black [25]). Hence, physical binding forces of Van der Waals type, that are relying on the pattern of inter-particle distances, provide an important contribution to material strength. Experimental studies into the structural features of the ITZ are difficult, time-consuming and liable to yield biased information [26,27]. Hence, computer-simulation could offer an attractive alternative. This is pursued in the forthcoming example of an application of the SPACE system to particle packing problems on micro-level. To describe such packing characteristics, a distinction should be made between composition and configuration [28-30].

4.1 Composition Gradient in the ITZ

Figure 8 offers information on an interesting effect of the packing of particles near a rigid boundary, *i.e.* size segregation.

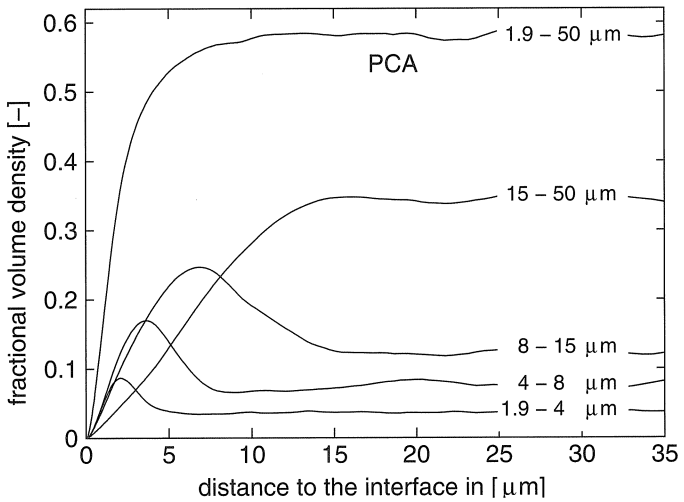

Figure 8: *Volumetric density of different size fractions of particles from model cement PCA, plotted as function of the distance to the interface; data are the average of six simulations*

A model cement with particles between 1.9 and 50 μm is considered. Although the size range is limited because of computational reasons, this will not fundamentally change the size segregation phenomenon. The particle sizes are for demonstration purposes grouped into a number of classes. As demonstrated, the peak density is proportional to the average particle size in the class. In other words, the smallest particles concentrate near the rigid interface as a natural phenomenon. For composition effects only the total volume fraction curve is used, however.

Figure 9 presents the Particle size Distribution Functions (pdf's) and Blaine numbers of the model cement pastes PCA and PCC that have been used throughout the remainder of this section. Note that the Blaine numbers are relatively low, because of the cut off limit in the lower size range. The pdf of the model cements is made to closely match the Rosin-Rammler curve, $G(d) = 1 - \exp(-bd^n)$, n and b being constants with values n=1.3, b=0.0175 for PCA, and n=1.4, b=0.033 for PCC [9,15]. The Rosin-Rammler curve is generally accepted to represent the particle size distribution of ordinary Portland cements. The well-established *Hymostruc* system [15] for simulation of hydration and structure formation is based on a similar concept (same pdf of spherical particles).
The volume fraction of particles in the ITZ is analysed for step-wise reduced water to cement ratios in the range from 0.6 to 0.2. To do so, a total of 10,000 spherical grains were dispersed in a cubic container of which the size was gradually reduced up until the desired water to cement ratio was reached. The bulk value of volume fraction is used to normalise the data. This total number of grains ensures that the number of larger particles in the model cement is so large that the actual pdf does not seriously deviate from the (truncated) continuous Rosin-Rammler function. Increasing the maximum grain size would require to proportionally increase the container size. The effect would be to the third power on the total number of particles. Despite economic algorithms in SPACE that avoid considering the position of all particles in studying the 'neighbourhood' of an arbitrary particle, which would have a very significant effect on computation time. Results are obtained by an *automated analysis of serial sections* parallel to the interface surface, discussed later.

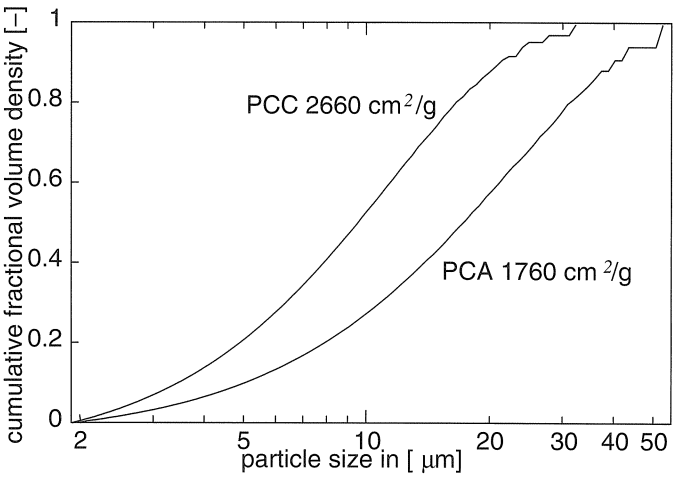

Figure 9: *The particle size distribution functions of model cements PCC and PCA, that are at the basis of the simulations of Figs. 8–14.*

Stereological interpretation yields the 3-D density information plotted as function of the distance to the interface. *Note that all data represent the average of six simulations.*

Figure 10 demonstrates an increase of the ITZ's thickness with increasing value of the water to cement ratio. The parameter at issue is the local value of particle volume fraction normalised by its bulk value. This is a composition criterion. Thickness of the ITZ is increased over the full range of water to cement ratios by a factor of about 2 [9]. More accurate estimates could be obtained by increasing the number of simulations and averaging the data, but main purpose here is to reveal *trends*.
Figure 11 reveals the change in ITZ thickness due to cement fineness for a paste with a water to cement ratio ratio of 0.2. Data are normalised by the respective bulk values of volume fraction. Additionally, porosity (interpreted here as complementary to particle volume density) declines significantly faster away from the interface in case of the finer cement. It can be expected that the addition of fine mineral admixtures such as silica fume will significantly enhance this rate in porosity decline in the vicinity of the interface.

4.2 Configuration Gradient in the ITZ

The curves of the various size classes in Figure 8 demonstrate the particle grading to change over a larger distance away from the interface than reflected by the total volume fraction curve [31]. This is a direct effect of the size segregation phenomenon.
Configuration in fine particle packing systems is important because of physical contributions to crack initiation strength or even to tensile strength. These contributions have been proven very significant even in the hardened state [24]. The most relevant parameter would be the distribution function of the surface-to-surface spacing to the nearest neighbour particle, $f(\Delta_3)$, expressed as a function of the distance to the interface, but for the present purpose this is too complicated. Instead, the *mean* free spacing, λ in μm is used. Although a three-dimensional parameter defining the *average* of all *unobstructed* surface-to-surface distances to neighbouring particles [32] is rather complicated to measure, it can easily and unambiguously be determined in sections, *i.e.*
$\lambda = 4(1 - V_V)/S_V$, whereby S_V is the specific surface area of the particles, and V_V the

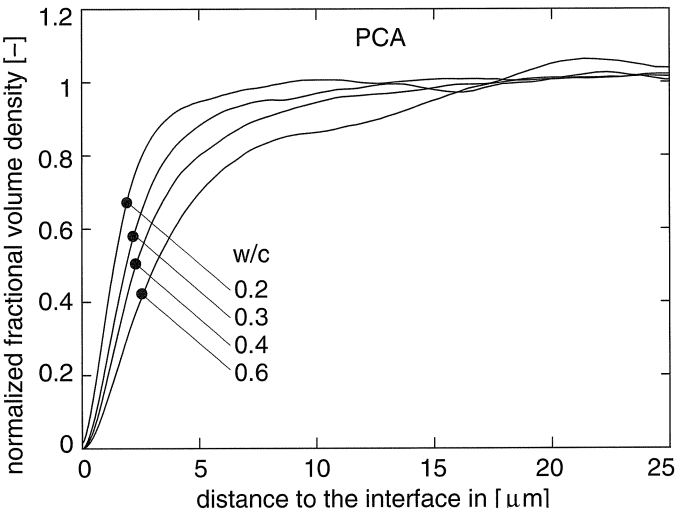

Figure 10: *Effect of water to cement ratio of the model cement paste (PCA) on volume density of the paste as function of the distance to the interface. The average results of six simulations are normalised by the bulk value of volume density.*

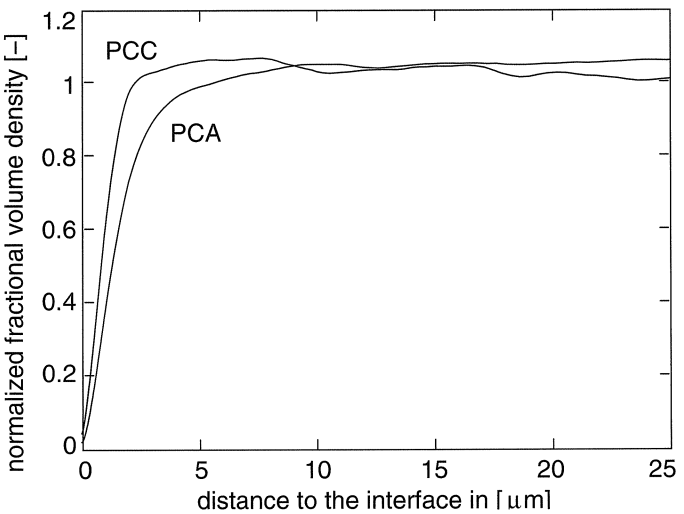

Figure 11: *Effect of the fineness of the model cement paste (PCA versus PCC) on the volume density gradient over the ITZ. The average results of six simulations are normalised by the respective bulk values of volume density (W/C=0.2).*

volume fraction. The total perimeter length of the circular cross-sections of the particles per unit of area in the section plane, L_A, is related to the surface area per unit of volume by $S_V = \frac{4}{\pi} L_A$. This allows for an unbiased and exact estimation of λ. The mean free spacing was employed earlier by Stroeven for the *experimental* assessment of particle packing characteristics in concrete [30]. It should be noted here, that the averaging procedures (in this case over distances to more neighbours, instead of using only the minimum value) reduces the configuration-sensitivity. Hence, structural effects revealed in forthcoming pictures will certainly not exaggerate the fundamental difference between composition and configuration homogeneity.
Under the assumption that physical strength (due to van der Waals-type of bonding forces) would be proportional to λ^{-3}, this parameter can be used to investigate effects of technological parameters on a moderately structure-sensitive parameter like this 'global bond strength'. Figs. 12 to 14 deal with effects of water to cement ratio and fineness of the binder on the global bond strength. The same PCA and PCC as defined in Figure 9 are employed for this purpose.

Figure 14 presents data normalised by the relevant bulk values. Hence, sufficiently far away from the interface the ordinate value is 1 (apart from statistical variation). With a reduction in water to cement ratio, the inter-particle bond capacity rises steeper in the immediate vicinity of the interface to a level that at lower water to cement ratios even exceeds bulk value. Hence, also the bond between the cement particles and the aggregate surface will increase proportionally. At increasing distance to the interface, unit value is gradually approached. The disproportional improvement of bond in the part of the ITZ immediately neighbouring the interface surface is restricted to the range of W/C=0.2 to 0.3 (relevant for HPC). This is accompanied by a significant *increase* in the ITZ thickness.

Figure 12 presents data of the fine-grained cement. The disproportional bond strength increase in the ITZ neighbouring the interface becomes already apparent at W/C=0.4. The strength increase is more dramatic than in case of the coarser model cement (PCA) (Figure 13). The latter effect is clearly revealed by Figure 14 that presents the global bond capacity data normalised by the relevant bulk values. Data are pertaining to the two model cements used in pastes with a water to cement ration of 0.2. Size segregation causes an accumulation of the smaller particles close to the interface (as demonstrated in Figure 8). This gives rise to a more rapid growth in inter-particle bond to a level that is 2.25 times exceeding the bulk property. This is about 40% exceeding the peak bond level of the PCA paste. Hence, selecting a fine-grained cement (larger Blaine number) or adding a mineral admixture with particles smaller than those of the cement (silica fume) will lead to a similar size-segregation phenomenon and a further disproportional improved bond capacity. A comparison between Figs. 12 and 13 learns the average level of the plotted parameter (that is supposed to be proportional to a global bond capacity) to be in all cases on a significantly higher level for the fine-grained model cement (PCC). The ITZ thickness increases with reduced water to cement ratios and is of the order of maximum grain size in the model cement for W/C=0.2. Hence, the extent of the ITZ depends on the composition of the material (W/C ratio) and on the position of the measuring parameter in the range between composition and configuration. The latter conclusion can be derived from a comparison of similar cases.
Note that the centre of the smallest particles in the mixtures will be at least at a distance of 1 μm from the interface. Maximum bond capacity of the finest cement (PCC) is attained at a distance of about 2.5 μm. In case of the second cement (PCA), this is about 4 μm. Hence, the building up of maximum bond capacity takes place over distances of approximately 1.5 μm for PCC and 3.0 μm for PCA, respectively; a difference of 100%. Since inter-particle

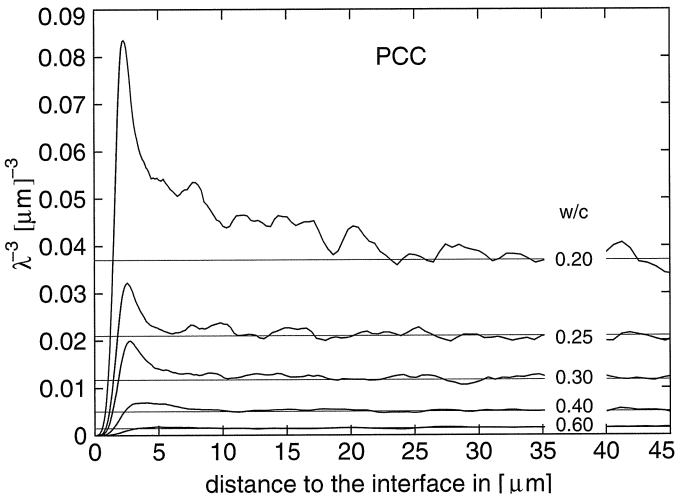

Figure 12: *Parameter proportional to global bond capacity in the ITZ as function of the water to cement ratio (PCC); λ=mean free spacing in µm. The average results of six simulations are presented.*

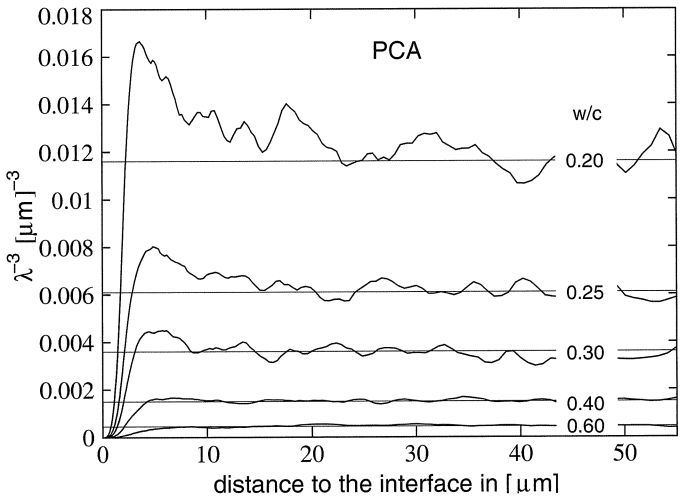

Figure 13: *Parameter proportional to global bond capacity in the ITZ as function of the water to cement ratio (PCA); λ=mean free spacing in µm. The average results of six simulations are presented.*

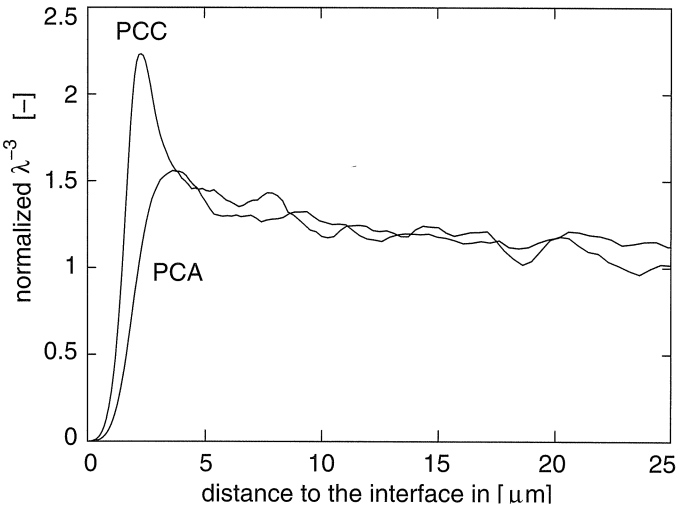

Figure 14: *Data of Figs. 13 and 12 with W/C=0.2 normalised by the respective bulk ordinate values. λ=mean free spacing in µm. The average results of six simulations are presented.*

distances in the layer immediately bordering the interface will be similar to particle-interface distances, the same conclusion can be drawn as to the level of physical bond between the particles and the interface surface.

Although not targeted in this paper, it would be of interest to see whether the gap can be bridged between experimental data and the presented simulation results on model cements. The SPACE system allows assigning forces to the particles in the dynamic stage of the simulation process to more closely simulate aggregation mechanisms, such as flocculation. Particle shape could be remodelled, although computational efforts for 'contact detection' will increase significantly. But, of course, simulating material structure inevitably asks for making structural simplifications. Nevertheless, the detection of trends in the aggregation of particular matter can be accomplished in a relatively easy way, whereby outcomes can be checked by comparison with actual measurements. The SPACE system provides a couple of additional parameters (like internal energy dissipation during the dynamic stage) that influence the aggregation process. For examples, see [9]. This would allow narrowing the gap between a real material and a model 'material' in a specific situation.

In comparing ITZ measurements on real materials and simulation data, we should account for the larger size range of real cements. This will exert a direct effect on the ITZ's extent (see, *e.g.* Figure 8). For the sake of the argument, proportionality is therefore assumed between the ITZ's thickness and the maximum grain size. For a cement with a noticeable fraction of grains in the 80 to 100 μm size range, this would lead to a roughly 20 to 25 μm thick ITZ shell for composition, and an 80 to 100 μm one for configuration. Of course, water to cement ratio and fineness of the binder will influence these data in a moderate way for composition measurements, and strongly for configuration parameters, as demonstrated herein. In comparing with experimental data, we have to acknowledge that experimental data on the ITZ's thickness may reflect other mechanisms than 'packing', although a common one as interface bleeding is probably of minor importance in the HPC

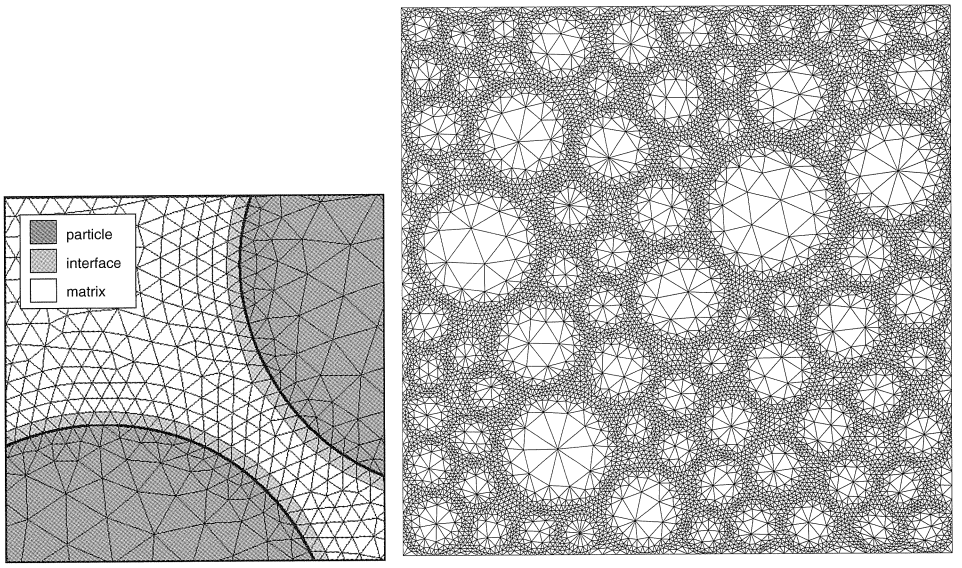

Figure 15: *Three material components are incorporated in the unstructured finite element mesh – close-up (left) and full-size view (right)*

range. Finally, experimental observations cannot easily be obtained on ITZ sections perpendicular to the aggregate grain's surface, leading to *biased* information. Even averaging over a series of random observations on apparent ITZ sections in a single large-scale section of the specimen would lead to estimates about 50% too large [26]. A general but fundamental problem is that the ITZ has no clear and obvious boundaries. Determination of the ITZ's thickness from gradient measurements, either experimental or simulated ones, can therefore neither be very accurate nor completely objective. Of more importance is therefore the recognition that the extent of the ITZ, though hard to delineate, will depend on material composition, as well as on the degree the parameter being studied is depending on material configuration. This phenomenon has been highlighted in this paper. The reader is referred for a more thorough treatment of this subject to a recently published paper of the authors [33].

5. Cracking in concrete

Recently, SPACE has been extended with the possibility to generate unstructured finite element meshes in which the material structure is explicitly modeled. Currently, only 2D meshes can be generated. Within these meshes, three components can be distinguished: aggregates, the cement matrix and the interfacial transition zone (the thin cement layer around each particle in which mechanical properties are different from that in bulk cement). In figure 15 part of a larger mesh is shown in which all three components can be distinguished. These meshes can be constructed because SPACE provides a full description of the material structure. Consequently, it is possible to provide the mesh generator with a function that defines the element size as a function of the distance to the nearest aggregate surfaces, for example. In this way, the interfacial transition zone (ITZ) – important for many mechanical properties in concrete – can be modeled with relative small elements while the elements within aggregates can be taken much larger.

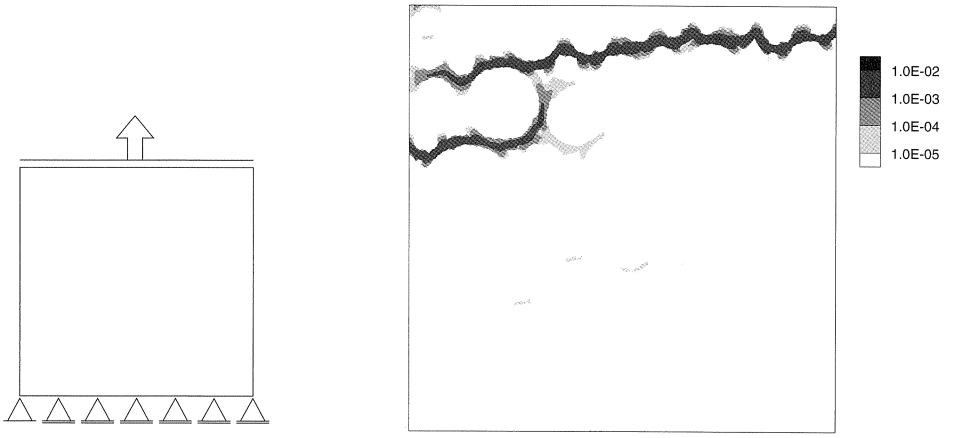

Figure 16: *The set up of the numerical tensile test* ***(left)*** *and the simulated (inelastic) strain contours in one of the specimen under direct tensile stresses* ***(right)***.

A series of two-dimensional aggregate structures have been generated, using two different size distributions. These are denoted (A) and (B) in Figure 17 (left). In series (A), size ranged from 1 to 4 mm, whereas in series (B), only sizes between 2 and 4 mm were considered. The particles were dispersed by the SPACE system over a square area of dimensions 14x14 mm. Thereupon, the particles were slightly eroded to create enough space between interconnected particles for the mesh generator to produce acceptable elements. The resulting areal fraction equalled 0.7 for all specimen in both series. These particle structures have subsequently been used to construct finite element meshes such as the one shown in Figure 15 (right).
Static tension experiments have been simulated on these square specimens of which the boundary conditions are depicted in Figure 16 (left). A vertical displacement was imposed on the upper side. In the present study, no periodicity of the boundary conditions is taken into account, and no periodicity of the microstructure is considered.
The assumed elastic parameters and the elastic threshold of the three phases are given in table 1. In order to model microcracking, all three materials have been modeled with a nonlocal damage model, see [34]. Thus, the mathematical formulation remains well-posed in the strain-softening regime. The nonlocal damage model incorporates an additional material parameter, usually denoted as the internal length scale. This internal length scale is supposed to represent the effects of a lower scale of observation. Normally, nonlocal damage models are used at a macroscopic scale and the internal length scale is used to account for mesostructural phenomena. However, here our observations take place on the mesoscale, so that the internal length scale must be interpreted as a manifestation of a lower (say, microscopic) scale. Given the heterogeneity of, for instance, cement paste (which constitutes of hydrated grains), this seems to be a valid assumption.

For all three material phases, the value of the internal length scale is set equal to the average element size in the ITZ. This implies that the microcracks initiated in the ITZ will

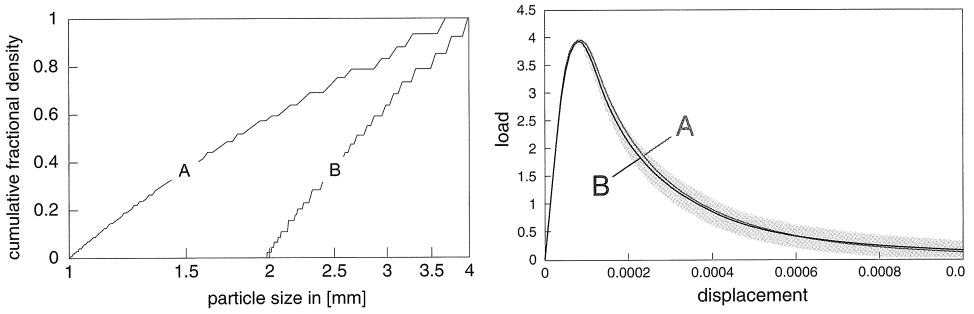

Figure 17: *Cumulative fractional density curves of the* A *and* B *series* ***(left)*** *and the load-displacement curves of simulated response in direct tension of specimens containing aggregate with different size distribution* ***(right)****. Scatter band of case* (B) *outcomes is additionally indicated.*

be distributed over a few elements around the ITZ. For an accurate representation of the microcrack it would have been necessary to use smaller elements, however this would have prohibited computer simulation due to storage and CPU times. For the present purpose of investigating RVEs, the relative coarseness of the finite element mesh is acceptable. In this context, it is noted that the internal length scale for the aggregates is much smaller than the applied element sizes for the aggregates, so that the regularizing effect of the nonlocal damage model would be lost in the aggregates. However, with the chosen elastic thresholds for aggregates, cracking does not occur in the aggregates. in Figure 16 (right) a typical contour plot of the equivalent strain is presented.
As can be seen from this figure, the (inelastic) strains concentrate in the ITZ. The load-displacement curves represent global behaviour. Figure 17 (right) presents the relevant curves of series (A) and (B) and the variation among the repeated simulations of series (B). Since the averages of the two series virtually coincide, the size distribution is obviously of little importance, provided total volume fraction of the mixtures is kept constant. Under the assumption that the post-peak load at complete fracture surface is primarily governed by the total surface area of the fracture plane, this finding would be in agreement with theoretical predictions, revealing indeed independence of the sieve curve [35,36].

6. Hydration of cement

Another interesting field for application of computer-simulation systems is cement hydration. To allow for realistic explorations of the structural implications of the

Table 1: *The various material parameters used for the tension experiments*

component	Young's modulus [N/mm^2]	Poisson ratio [-]	crack initiation strain [-]
matrix	35.000	0.2	1e-4
ITZ	35.000	0.2	1e-5
aggregates	100.000	0.2	2e-4

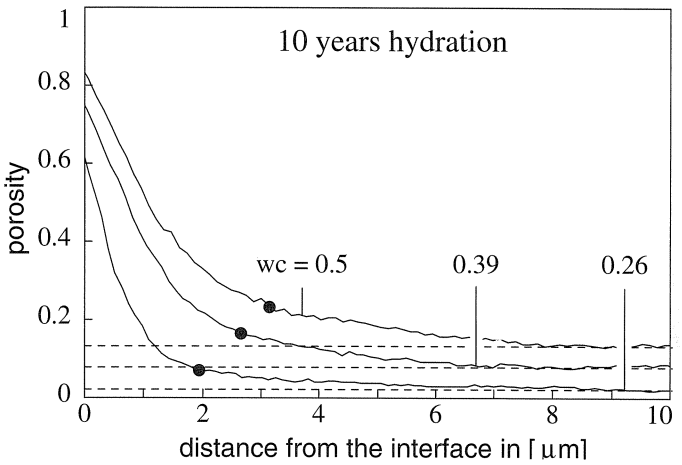

Figure 18: *Porosity gradient in ITZ for different W/C ratios after 10 years of hydration.*

hardening phenomenon, 'hydration' has been implemented in SPACE. As to the validity of the approach, reference can be made to a close correspondence found between the measured strength development of hydrating cement pastes by Locher [37] and SPACE simulations for pastes with three different water to cement ratios (*i.e.* W/C=0.26, 0.388 and 0.50), assuming the strength development to be proportional to the growing contact surface area per unit of volume [9].
Preliminary results [9,38,39] obtained by means of SPACE simulations revealed maturity to have opposite effects on normal concretes and on HPCs; at low water to cement ratios, the ITZ thickness declined somewhat with maturity, whereas an increase was detected for normal concrete (W/C>0.42)) [9]. However, the gradient pattern of the particle packing stage is not changing *fundamentally*, as can be seen also in Figure 18.
The effect of water to cement ratio on configuration is significant, as we have seen before. This leads during hardening to dramatic effects. By reducing the water to cement ratio from 0.5 to 0.4, image patterns made at 10 years hardening revealed a connected pore structure (Figure 19 (right)) to transform into a disconnected network in bulk of the model material (not shown) [9,40]. This subject will be more elaborately discussed in a forthcoming PhD study (by Hu Jing), pursuing among other things the characterisation of pore structure by modern geometrical statistical methods of stereology and of mathematical morphology. A further reduction in the water to cement ratio from 0.4 to 0.26 yielded the number and total volume of anhydrous cement particles to increase disproportional. This phenomenon is presently subjected to a more elaborate study with the help of SPACE in the framework of a Dutch-Chinese co-operation programme on 'Modern Concrete Composites'. Distributions of pore clusters and of anhydrous cement particles showed a large degree of inhomogeneity. This conforms to experimental observations published in the literature [27,41,42]. The explanation is the configuration-sensitivity of both phenomena. The higher porosity in the ITZ causes a significant reduction in the anhydrous cement content, but the gradient will still be governed by configuration. Hence, the ITZ's thickness based on the anhydrous cement content homogeneity will exceed the one for composition considerably. This is also confirmed by Diamond and Huang [41].

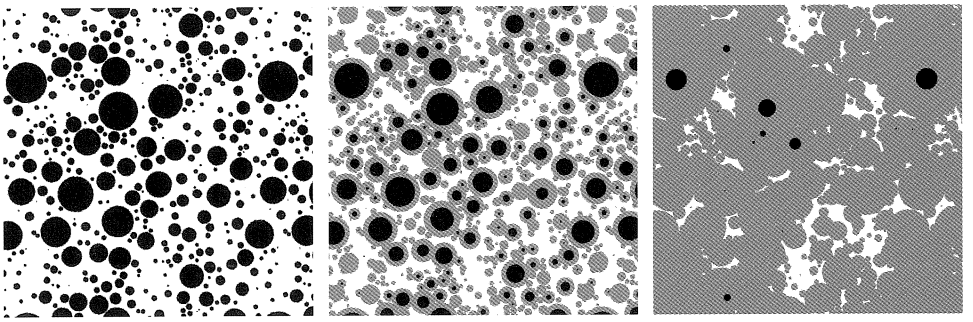

Figure 19: *Sections of bulk cement paste with W/C=0.5 during hydration;* ***(left)*** *initial stage,* ***(middle)*** *after 3.2 days, and* ***(right)*** *after 10 years of hydration (white areas indicate water/air, grey areas represent gel and black areas correspond to unhydrated cement.)*

7. Conclusions

Particle packing problems on different levels of the microstructure, ranging from maximum attainable density of gravel and sand mixtures on meso-level, to particle density distributions of cement and mineral admixtures on micro-level (as in the ITZ), can be approached effectively by the SPACE system. So far, particles are assumed spherical, so that shape effects are excluded. In the future, the system will be expanded to estimate mechanical or physico-chemical properties by incorporating the appropriate properties on microlevel.

The combination of a flexible software package combined with modern computer graphics techniques provides an excellent tool for simulating a variety of material systems, as shown for concrete on various levels of the microstructure. This renders possible the investigation of 'actual' structural material properties in 3-D space. The system is versatile. By changing the element properties and interactions, in principle a wide variety of engineering materials can be studied. An example in the field of cementitious materials is the effect of a superplasticizer on the distribution of cement particles in the fresh mix.

The effects of implemented mechanisms should be validated by experiments. Since this contribution aimed at illustrating the capabilities of SPACE for studying structural phenomena due to particle packing on different levels of the micro-structure, this topic was not touched upon. So far, validation has been accomplished on mono-sized particle packings compacted to maximum density, and on strength development during hydration of model cement pastes [9]. For both cases, experimental data were available. The application to optimisation of gravel, or gravel and sand mixtures, presented herein, constitutes another case of validation.

SPACE simulations on model cements clearly revealed the trends due to global changes in the water to cement ratio and the cement fineness on the gradient in volume fraction of the cement particles in the ITZ. The thickness of the ITZ was in all cases only a portion of the maximum grain size of the model cement, in agreement with experimental evidences. The investigated volume fraction parameter measures *composition* of the simulated cement structure.

Contrarily, the discrimination to separate particle fractions in the SPACE approach, shows the discontinuity in particle *configuration* to extend inwards over a depth considerably exceeding the one in volume density. This phenomenon is denoted as size segregation. Since *structure-sensitive properties* depend on the details of particle packing, account should be given to a relatively wide interphase zone in assessing such material properties (like

resistance to crack initiation and early crack propagation). Also on macrolevel, the discontinuity in aggregate grading (or spacing) will extend considerably more inward than estimated by volume density of the aggregate. This is in agreement with experimental evidence [30].
Simulation of configuration homogeneity for densely packed particles can not be accomplished without significant biases by conventional random generator-based systems. The paper introduces for illustrative purposes a 'global bonding capacity', as an example of a medium configuration-sensitivity property. The more dramatic effects on this bonding capacity inside the ITZ due to changes in the W/C ratio, and in the cement fineness are highlighted. Particularly under conditions relevant for HPC (W/C=0.2, finest cement), the bonding capacity is *disproportional improved* due to size segregation. The associated ITZ will have a thickness of the order of maximum grain size of the cement.
The *ITZ has no distinct boundaries* due to the gradual transfer to bulk features. Deriving the thickness of the ITZ for a given composition and for the associated parameter of interest from gradient structural information would be equally difficult for experimental and simulated data. Moreover, experimental observations will suffer from a low-sensitivity (so, large scatter), and mostly be more seriously biased [26].

8. References

1. Stroeven, M., Stroeven, P. Computer-simulated internal structure of materials. Acta Stereol, 15, 3, 1996, pp. 247-252.
2. Hsu, T.C., Slate, F., Sturman, G., Winter, G. Microcracking in concrete and the shape of the stress-strain curve, J. ACI, 60, 2, 1963.
3. Pigeon, M. The process of crack initiation and propagation in concrete, PhD Thesis, Imperial College, London, 1969.
4. Mc Greath, D.R. The fracture mechanics of concrete, PhD Thesis, Imperial College, London, 1968.
5. Zaitsev, J.W., Wittmann, F.H. Crack propagation in a two-phase material such as concrete, Fracture 1977, Vol. 3, ICF4, Waterloo, Canada, June 19-24, 1977, pp. 1197-1203.
6. Stroeven, P. Crack development in concrete as influenced by the addition of short steel fibres. Fracture Mechanics, Proc. Symp. Delft, Delft Univ. Techn., Delft, 1979.
7. Stroeven, P., Guo, W. Structural modelling and mechanical behaviour of steel fibre reinforced concrete. Fibre Reinforced Cements and Concretes, Recent Developments, Swamy, R.N., Barr, B. (eds), Elsevier Appl. Sc., London, 1989, pp. 345-354.
8. Guo, W., Stroeven, P. The analysis of wire distributions in computer-simulated wire-reinforced materials, Acta Stereol., 8/2, 1989, pp. 683-688.
9. Stroeven, M. Discrete numerical model for the structure assessment of composite materials, PhD thesis, Delft Univ. Techn., Delft, 1999.
10. Stroeven P, Stroeven M. Micromechanical behaviour of concrete interpreted by computer simulation system for material structure. Computational Methods and Experimental Measurements IX. G.M. Carlomagno, C.A. Brebbia (eds), WIT Press, Southampton, 1999, pp. 571-582.
11. Roelfstra, P.E. A numerical approach to investigate the properties of numerical concrete, PhD Thesis, EPFL-Lausanne, Lausanne, 1989.
12. Diekkämper R. Ein Verfahren zur numerischen Simulation des Bruch- und Verformungsverhaltens spröder Werkstoffe, Techn. Wissenschaftliche Mitteilungen der Institut für Konstruktiven Ingenieursbau, Ruhr Universität Bochum, 7, 1984.
13. Bentz, D.P., Garboczi, E.J., Stutzman, P.E. Computer modelling of the interfacial zone in concrete. Interfaces in Cementitious Composites, Maso, J.C. (ed), E & FN Spon, London,

1993, p. 107-116.
14. Brach, R.M. Mechanical Impact Dynamics, Rigid Body Collisions, John Wiley & Sons, New York, 1991.
15. Breugel, K. van. Simulation of hydration and formation of structure in hardening cement-based materials. PhD Thesis, Delft Univ. Techn., Delft, 1991.
16. Silla, E., Tuñón, I., Pascual-Ahuir, J.L.
GEPOL: An improved description of Molecular surfaces II. Computing the molecular area and volume, J. Comp. Chem., 12, 9, 1991, pp. 1077-1088.
17. Donker, L., Experimental assessment of optimum density of sand/gravel mixtures, Report 03.21.1.32.12 Delft Univ. Techn., Faculty of Civil Engineering, Delft, 1998 (in Dutch)
18. Toralles-Carbonari, B., Gettu, R., Agulló, L., Aguado, A., Aceña, V. A synthetic approach for experimental optimization of high-strength concrete. Proc. 4th Int. Symp. Utilization of High Strength Concrete, F. de Larrard, R. Lacroix (eds), Presse de l'école des Ponts et chaussées, Paris, 1996, pp. 161-167.
19. Sedran, T., Larrard, F. de. René-LCPC: software to optimize the mix design of high performance concrete. Proc. 4th Int. Symp. Utilization of High Strength Concrete, F. de Larrard, F., R. Lacroix (eds), Presse de l'école des Ponts et chaussées, Paris, 1996, pp. 169-178.
20. Study Centre for Road Construction, Various properties of natural sands for Netherlands highway engineering, Report Working Group F 4 'Sub-base', 14A Jansbuitensingel, Arnhem, The Netherlands, 1978.
21. Vieser, W., Proportioning concrete, Zement, Sept. and Oct., 1926.
22. Stroeven, P., Stroeven, M., Assessment of packing characteristics by computer simulation, Cem. Concr. Res., 29, 1999, pp. 1201-1206.
23. Jiang, W., Roy, D.M. Strengthening mechanisms of high-performance concrete, High Performance Concrete, Proc. ACI Int. Conf. Singapore, V.M. Malhotra (ed), ACI, Detroit, 1994, pp. 753-767.
24. Fidjestøl, P., Frearson, J. Highperformance concrete using blended and triple blended cements, High Performance Concrete, Proc. ACI Int. Conf. Singapore, V.M. Malhotra (ed), ACI, Detroit, 1994, pp. 135-157.
25. Detwiler, R.J., Metha, P.K. Chemical and physical effects of silica fume on mechanical behaviour of concrete, ACI Mat. J., 86, 6, 1989, pp. 609-614.
26. Stroeven, P. Analytical and computer-simulation approaches to the extent of the interfacial transition zone in concrete, Proc. Brittle Matrix Conference 6, A.M. Brandt, V.C. Li, I.H. Marschall, (eds), Woodhead Publ Co & Z Turek RSI, Cambridge, 2000, pp. 465-474.
27. Scrivener, K.L. The microstructure of concrete, Materials Science of Concrete I, J.P. Skalny (ed),, Americ. Ceram. Soc., Westerville (OH), 1989, pp. 127-161.
28. Freudenthal, A.M. The Inelastic Behavior of Engineering Materials and Structures, John Wiley & Sons, New York, 1950.
29. Holliday, L. Geometrical considerations and phase relationships, Composite Materials, L. Holliday (ed), Elsevier Publ. Co, Amsterdam, 1966, pp. 1-27.
30. Stroeven, P. Some Aspects of the Micromechanics of Concrete. PhD Thesis, Delft Univ. Techn., Delft, 1973.
31. Stroeven, P., Stroeven, M. SPACE simulation of particle packing in the ITZ; a spatial perspective on the ITZ's relevance, Proc. Int. Symp. High Performance Concrete - Workability, Strength and Durability I, Hongkong Univ. Science & Techn., Hongkong, 2000, pp. 509-514.
32. Fullman, R.L. Measurement of particle sizes in opaque bodies, Trans. Met. Soc. AIME, 197, March, 1953, pp. 447-452.
33. Stroeven, P., Stroeven, M., Reconstructions by SPACE of the Interfacial Transition Zone, Cem. Concr. Comp., 23, 2001, pp. 189-200.

34. Pijaudier-Cabot, G. and Bažant, Z.P., Nonlocal damage theory, ASCE Journal of Engineering Mechanics, 113, 1987, PP. 1512–1533
35. Stroeven, P., Stereological estimates for roughness and tortuosity in cementitious systems, Image Anal. Stereol., 19, 2000, pp. 67-70.
36. Stroeven, P., A stereological approach to roughness of fracture surfaces and tortuosity of transport paths in concrete., Cem. Concr. Comp., 22, 2000, pp. 331-341.
37. Locher, F.W. Die Festigkeit des Zements, Beton, 26, 8, 1976, pp. 283-285.
38. Stroeven, M., Stroeven, P. Simulation of hydration and the formation of microstructure, Computational Plasticity, D.R.J. Owen, E. Oñate, E. Hinton (eds), CIMNE, Barcelona, 1997, pp. 981-987.
39. Stroeven, M., Stroeven, P., SPACE system for simulation of aggregated matter; application to cement hydration, Cem. Concr. Res., 29, 1999, pp. 1299-1304.
40. Navi, P., Pignat, C. Simulation of cement hydration and connectivity of the capillary pore space, Adv. Cem. Bas. Mat., 4, 1996, pp. 58-67.
41. Diamond, S., Huang, J. The interfacial transition zone: reality or myth?", The Interfacial Transition Zone in Cementitious Composites, A. Katz, A. Bentur, M. Alexander, G. Arlinguie (eds), E&FN Spon, London, 1998, pp. 3-39.
42. Ollivier, J.P., Maso, J.C., Bourdette, B. Interfacial transition zone in concrete, Adv. Cem. Bas. Mat., 2, 1995, pp. 30-38.